Electronic supplementary information

Electrochemical Activity of 1T' Structured Rhenium Selenide Nanosheets via Electronic Structure Modulation over Selenium-Vacancy Generation

Yuan Sun,[abcd] Jie Meng,[ade] Huanxin Ju,[f] Junfa Zhu,[f] Qunxaing Li[ade] and Qing Yang*[abcd]

[a]Hefei National Laboratory of Physical Sciences at the Microscale, University of Science and Technology of China (USTC), Hefei 230026, Anhui, P. R. China.

[b]Department of Chemistry, USTC, Hefei 230026, Anhui, P. R. China.

[c]Laboratory of Nanomaterials for Energy Conversion, USTC, Hefei 230026, Anhui, P. R. China.

[d]Synergetic Innovation Center of Quantum Information & Quantum Physics, USTC, Hefei 230026, P. R. China.

[e]Department of Chemical Physics, USTC, Hefei 230026, Anhui, P. R. China.

[f]National Synchrotron Radiation Laboratory, USTC, Hefei 230029, Anhui, P. R. China

* E-mail: qyoung@ustc.edu.cn; Fax: +86-551-63606266; Tel: +86-551-63600243

1. Experimental Section

Materials Preparation: The $ReSe_{2-x}$ catalysts were prepared using a bottom-up hot-injection colloidal synthetic route by inspiration and modification of our recent work.[S1] The synthetic procedure was conducted under the protection of argon. First, 5 mL of oleylamine (OAm) in a three-necked flask was heated to 150 °C and maintained at the temperature for 20 min, then the temperature was raised to 320 °C. Then, 0.2 mmol of NH_4ReO_4 and a certain amount of dibenzyl diselenide ($(PhCH_2)_2Se_2$, 0.12, 0.15, 0.18, 0.20, 0.24 mmol) in 2

mL OAm were injected into the flask, and the mixture was kept at 315 °C for 30 min. Finally, the solution was cooled down to room temperature and the black products was separated by centrifugation. The products were washed with toluene for four times and dried at 70 °C for 6 hours.

$ReSe_2$ nanospheres were synthesized under the same conditions except that the 2 mL of OAm containing 0.2 mmol of NH_4ReO_4 and 0.3 mmol of $(PhCH_2)_2Se_2$ were injected into the reaction system for instead.

Electrochemical Measurements: Electrochemical measurements were performed in a three-electreode system on a CHI660E electrochemical workstation, using a Ag/AgCl (in saturated KCl sulution) electrode as the reference electrode and a graphite rod as the counter electrode. The working electrodes were prepared as follows: Firstly, the catalysts were cleaned with acetic acid, as reported,[S2] then the products were washed with ethanol for four times and dried at 70 °C for 6 hours. Afterwards, 20 mg of the prepared sample was dispersed in 1 mL of ethanol and 30 μL of the catalyst ink was drop-cast onto a carbon paper (0.5 × 0.5 cm^2), followed by drying in an oven at 70 °C. All cyclic voltammetry curves for the stability tests were recorded at a sweep rate of 50 mV s^{-1} and linear sweep voltammetry curves were recorded at 5 mV s^{-1} for the performance test. The electrochemical impedance spectroscopy measurement was performed at an overpotential of 100 mV from 10^6 – 0.01 Hz at the amplitude of 5 mV. All the potentials were calibrated with respect to the reversible hydrogen electrode (RHE): E(vs RHE) = E(vs Ag/AgCl) + 0.059 × pH + 0.197.[S3,S4]

Characterization: The structure and morphology of the as-obtained rhenium selenide nanomaterials were characterized by a Philips X'pert PRO X-ray diffractometer with Cu Kα, λ = 1.54182 Å, a JSM-6700F and a Hitachi H-7650 for SEM and TEM, respectively. The structure, microstructure and composition of the nanostructures were determined by HRTEM, high-angle annular dark-field scanning transmission electron microscopy (HAADF-STEM), elemental mapping and the corresponding energy-dispersive X-ray spectroscopic (EDX) mapping, performaned on a JEOL JEM-ARF200F TEM/STEM with a spherical aberration corrector. Elemental ratios were detected by inductively-coupled plasma atomic emission spectroscopy (ICP-AES) at Galbraith Laboratories (Knoxville, TN). Raman and photoluminescence spectra were recorded on a Renishaw inVia Raman system with an excitation wavelength of 785 nm. Meanwhile, high resolution synchrotron radiation photoelectron spectroscopy (HR-SRPES) and Ultraviolet photoelectron spectroscopy (UPS) were obtained from the Catalysis and Surface Science End station at the BL11U beamline in the National Synchrotron Radiation Laboratory (NSRL) in Hefei, China. HR-SRPES of Re 4f and Se 3d were acquired with photoelectron energy of 200 eV as the excitation source, and the UPS spectra were measured with photon energy of 40 eV using a bias of -5 V in order to observe the secondary electron cut-off. EPR spectra were measured on an EPR spectrometer (JEOL JES-FA200) at 300 K and 9.066 GHz. The specific surface area was measured with the BET (Brunauer-Emmet-Teller) method using a Micromeritic TriStar II 3020 V1.03 (V1.03) instrument (Micromeritics Instrument Corporation, USA).

2. Calculation details

Method: All density functional theory (DFT) calculations were performed using Vienna ab initio simulation package (VASP) [S5, S6]. Electron exchange and correlation were treated using the Perdew-Burke-Ernzerhof (PBE) [S7] form of the generalized-gradient approximation with van der Waals (vdW) correction proposed by Grimme, [S8, S9] due to its good description of long-range vdW interaction. A plane-wave cutoff energy of 400 eV was used and the Brillouin zone was sampled with a 10×10×1 k-point mesh. [S10] The convergence of energy and forces were set to be 1×10^{-5} eV and 0.02 eV, respectively. A vacuum region of around 12.0 Å was set along the z direction to avoid the interaction between periodic images. The optimized lattice constants of triclinic $ReSe_2$ monolayer were predicted to be a = 6.72 Å and b = 6.60 Å, which are close to the previous reported values (a = 6.742 Å, b = 6.697 Å). [S11, S12] In our calculations, a four-layer (4L) $ReSe_2$ model was adopted to describe the $ReSe_2$ nanospheres, where each layer of $ReSe_2$ consisted of 12 atoms (4 Re and 8 Se atoms). The $ReSe_{2-x}$ nanosheets were simulated as bilayer $ReSe_{2-x}$, in which each layer consisted of 4 Re atoms and 7 Se atoms. That is to say, one Se vacancy was included in each layer.

The free energies of adsorbed H (ΔG_{H*}) on different surfaces were calculated by using standard methods. [S13] The H adsorption free energy (ΔG_{H*}) was defined as $\Delta G_{H*} = \Delta E_{H*} + \Delta E_{ZPE} - T\Delta S_H$. Here, ΔE_{H*} is the H chemisorption energy, ΔE_{ZPE} is the difference in zero point energy, ΔS_H is the difference in entropy between the adsorbed and the gas phase, and T is the temperature (298 K). In our simulations, the H chemisorption energy (ΔE_{H*}) was defined as $\Delta E_{H*} = E_{ReSe2+H} - E_{ReSe2} - 1/2\ E_{H2}$, where $E_{ReSe2+H}$ and E_{ReSe2} are the total energy of the adsorption system (H adsorbed on $ReSe_2$ surface) and $ReSe_2$ substrate surface,

respectively, and E_{H2} stands for the energy of gas phase H_2 molecule. We performed normal mode analysis to determine the zero point energy correction, namely, ΔE_{ZPE} can be computed by $\Delta E_{ZPE} = E_{ZPE\text{-}H*} - 1/2E_{ZPE\text{-}H2}$. Due to the fact that the vibrational entropy can be neglected in the adsorbed state, [S10] ΔS_H can be approximated using $\Delta S_H \cong 1/2S^0_{H2}$, where S^0_{H2} is the entropy of H_2 in the gas phase at standard conditions.

The adsorption energies of H species (ΔE_{H*}), the relevant contributions to the free energy, and free energy of adsorbed H (ΔG_{H*}) were summarized in Table S1.

Table S1. The calculated ΔE_{H*}, ΔE_{ZPE}, $-T\Delta S_H$, and ΔG_{H*} (in eV).

Species	ΔE_{H*}	ΔE_{ZPE}	$-T\Delta S_H$	ΔG_{H*}
H_2	-	0.265	-0.20	-
H* on 2L-$ReSe_{2-x}$	-0.29	0.13	-0.20	-0.36
H* on 4L-$ReSe_2$	1.53	0.11	-0.20	1.44

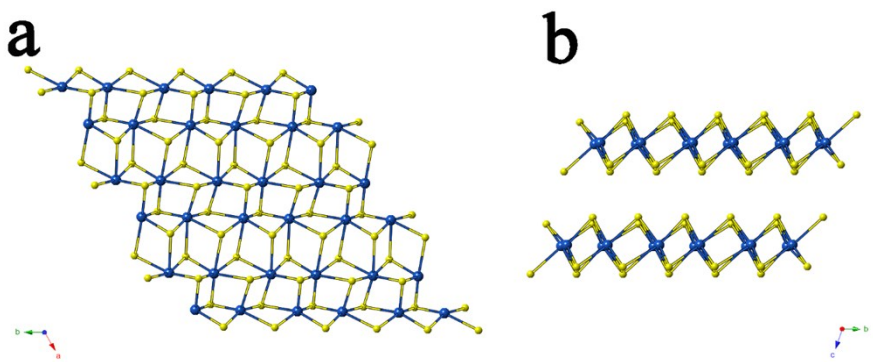

Fig. S1 Schematic diagram of ball-and-stick models of triclinic Re-based dichalcogenides (ReS_2 and $ReSe_2$) (a) view along [001] and (b) view along [100]. The Re atom and Se(S) atom are displayed in blue and yellow, respectively.

Table S2. Elemental ratios of the products prepared from different ratios of NH_4ReO_4 / $(PhCH_2)_2Se_2$

ratios of NH_4ReO_4 /$(PhCH_2)_2Se_2$	1:0.6	1:0.75	1:0.9	1:1	1:1.2	1:1.5
ICP-AES detected Re:Se mole ratio	1:1.04	1:1.20	1:1.27	1:1.68	1:1.87	1:2
contents of Se vacancy	48.8%	40.7%	36.0%	15.9%	6.6%	0

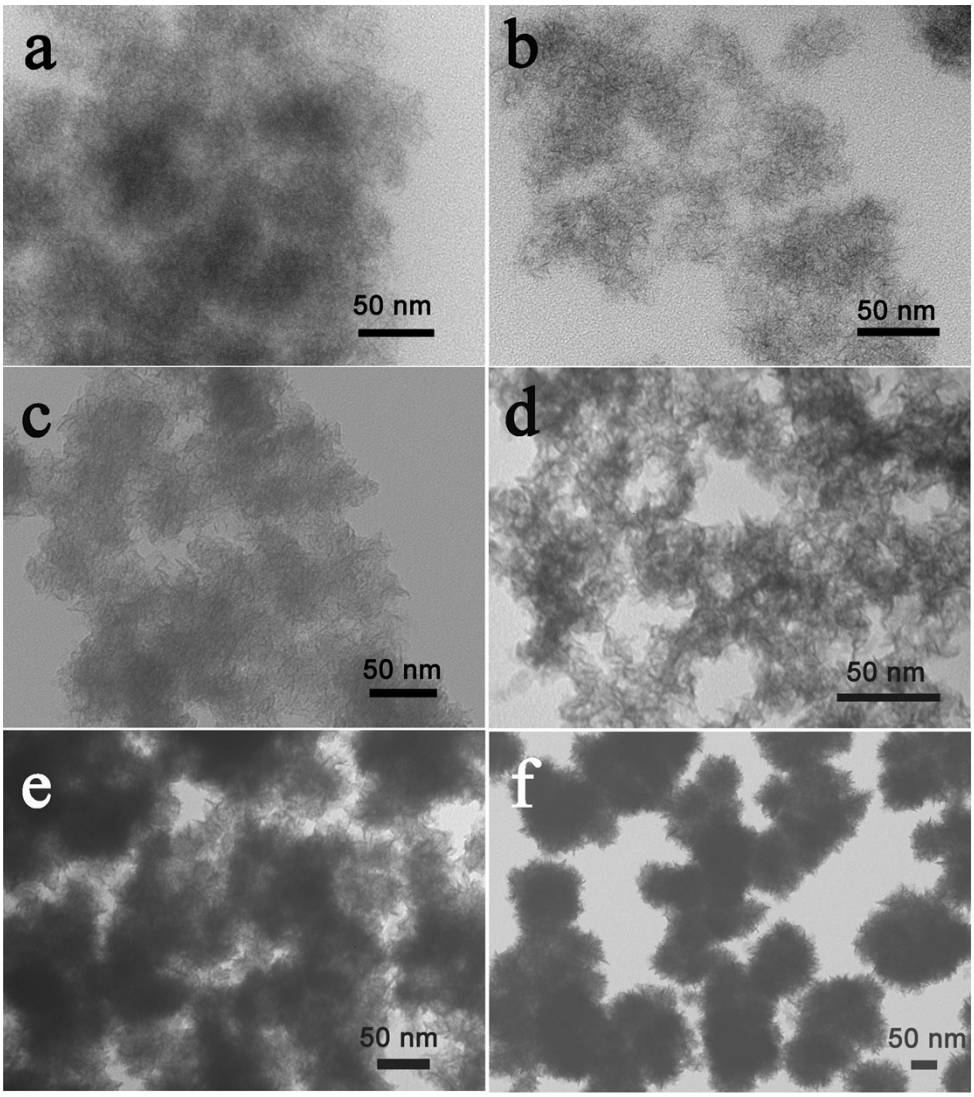

Fig. S2 TEM images of the products obtained from different ratios of NH_4ReO_4/ $(PhCH_2)_2Se_2$: (a) 1:0.6, (b) 1:0.75, (c) 1:0.9, (d) 1:1, (e) 1:1.2 and (f) 1:1.5.

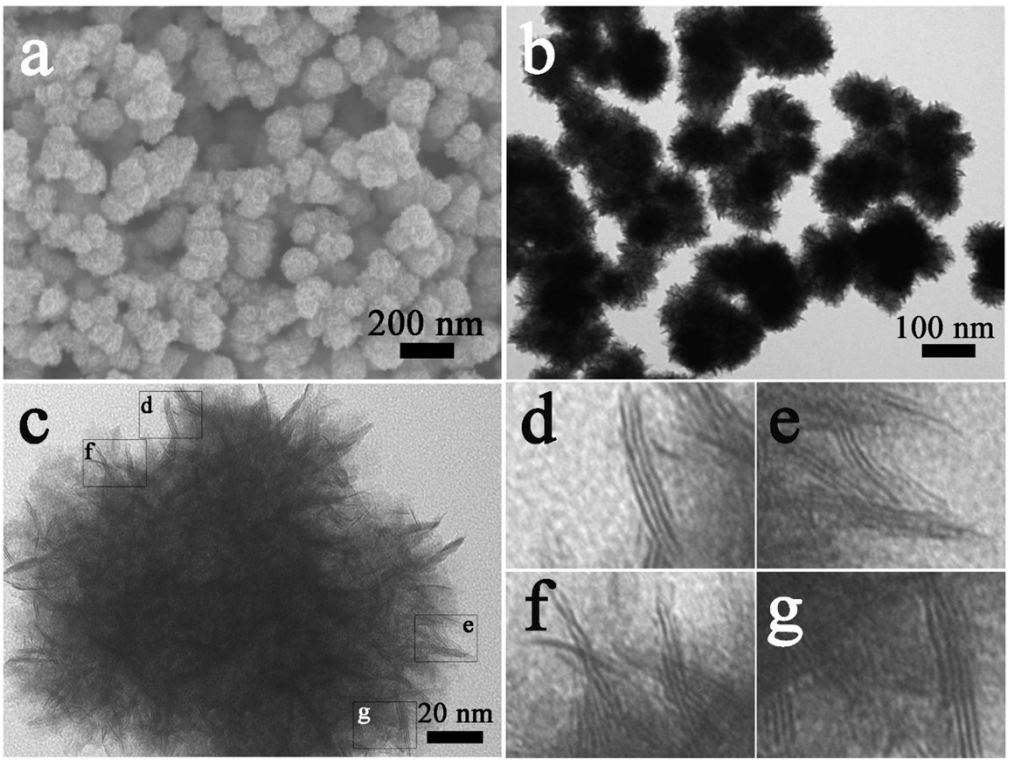

Fig. S3 (a) Scanning electron microscope (SEM) image, (b) TEM image, (c) high resolution TEM image, and (d-g) partial enlargements from (c) of the $ReSe_2$ nanospheres.

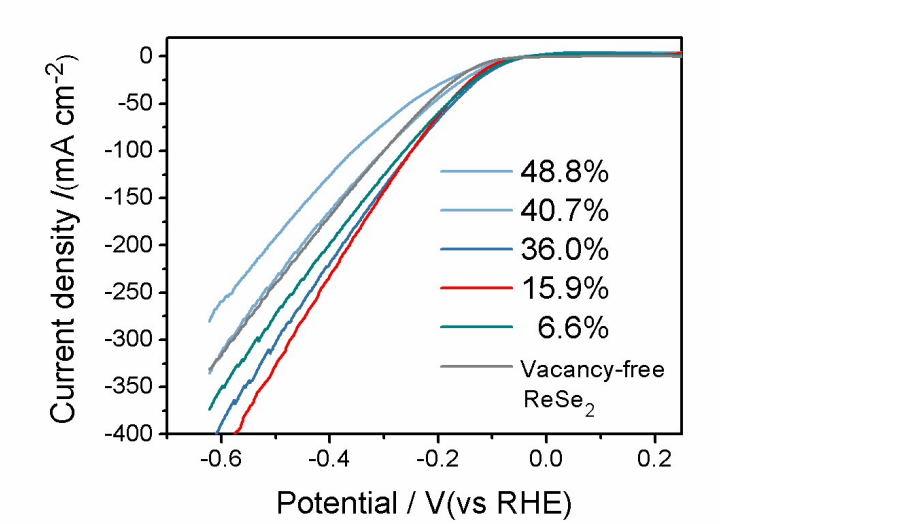

Fig. S4 LSV curves of $ReSe_{2-x}$ samples with different content of Se vacancy. The optimized concentration determined to be 15.9% in the present investigations.

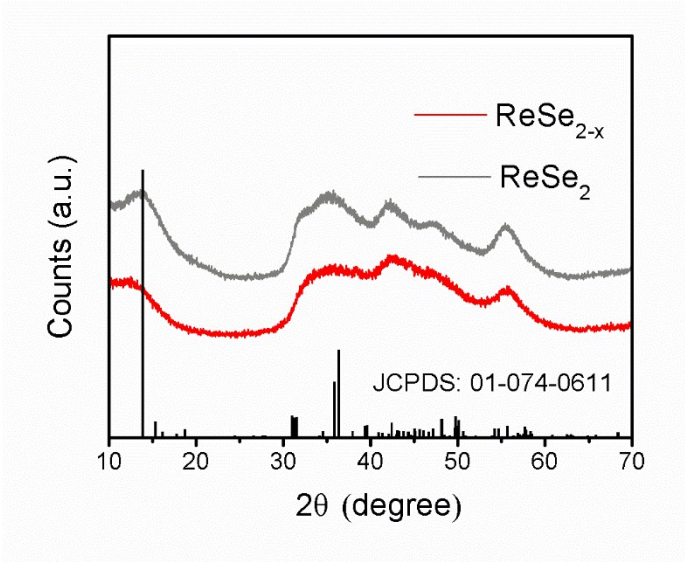

Fig. S5 X-ray diffraction (XRD) pattern of the as-synthesized $ReSe_{2-x}$ nanosheets and $ReSe_2$ nanospheres.

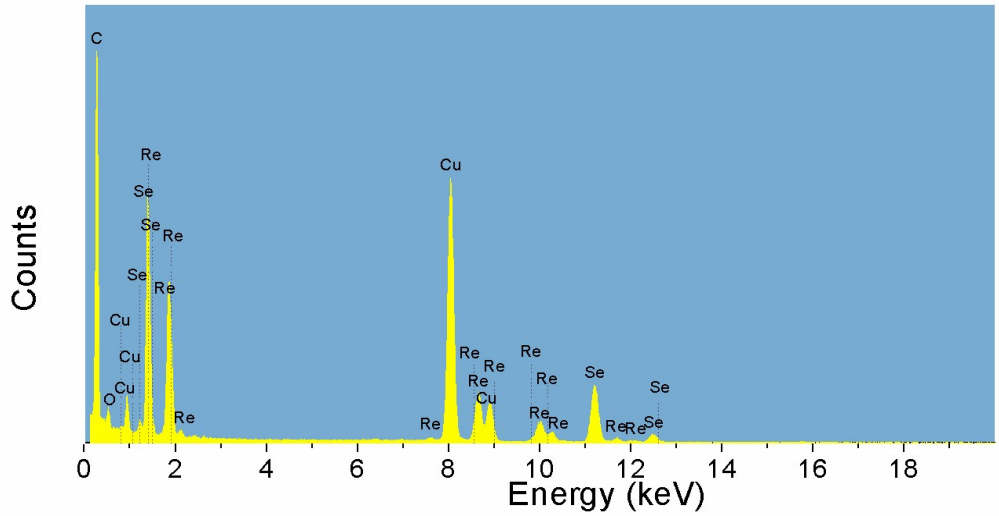

Fig. S6 EDX spectrum of the $ReSe_{2-x}$ nanosheets. The signal of Cu and C arises from the TEM grid made of Cu grids and carbon film.

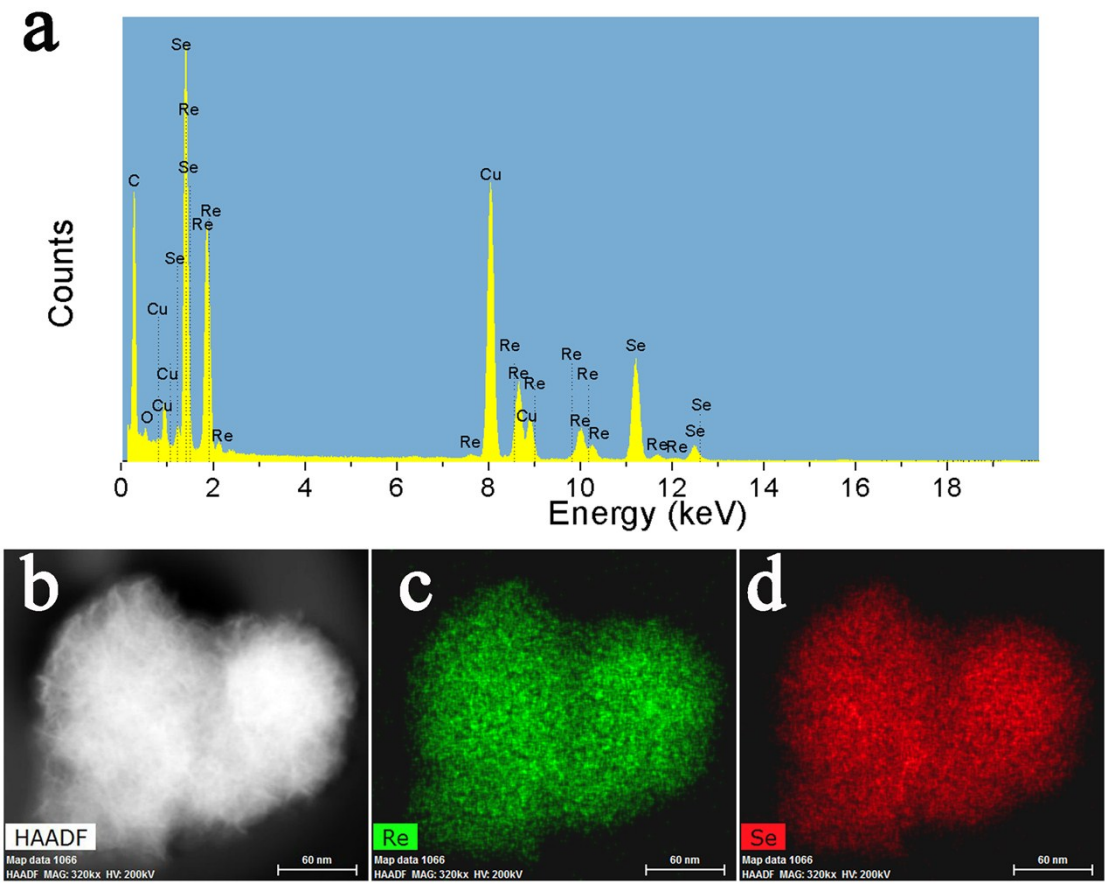

Fig. S7 (a) EDX spectrum of the $ReSe_2$ nanospheres, (b) HAADF-STEM image and (c) and (d) the corresponding EDX mapping images of the as-synthesized $ReSe_2$ nanospheres. Element Re and Se both distribute homogenously in the sample.

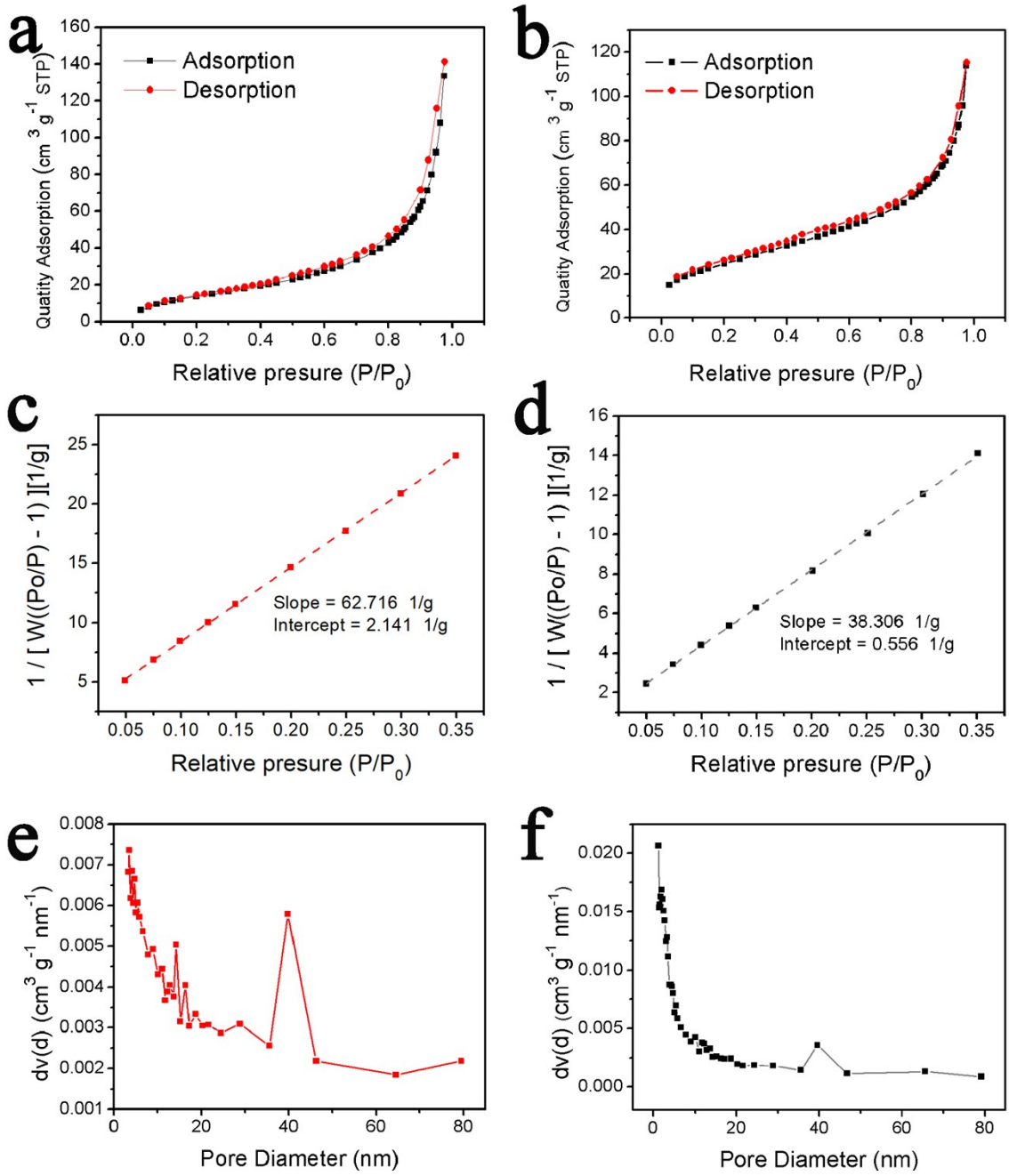

Fig. S8 (a) N_2 adsorption/desorption isotherms, (c) multi-point BET plot, and (e) pore size distribution of the $ReSe_{2-x}$ nanosheets, (b) N_2 adsorption/desorption isotherms, (d) multi-point BET plot, and (f) pore size distribution of the $ReSe_2$ nanospheres. The multi-point BET surface area, BJH adsorption pore volume and pore diameter are 53.696 m^2/g, 0.215 cm^3/g and 3.512 nm for the $ReSe_{2-x}$ nanosheets and 89.611 m^2/g, 0.185 cm^3/g and 1.194 nm for the $ReSe_2$ nanospheres, respectively.

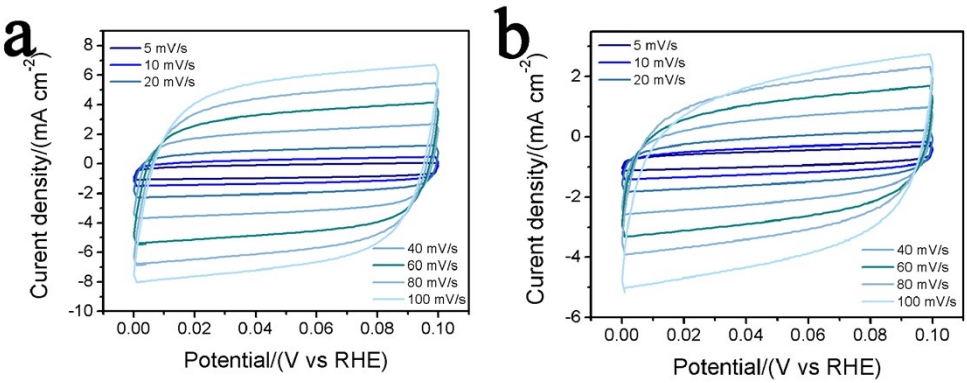

Fig. S9 CV curves of (a) the $ReSe_{2-x}$ nanosheets, and (b) the $ReSe_2$ nanospheres in the region of 0-0.1 V vs. RHE.

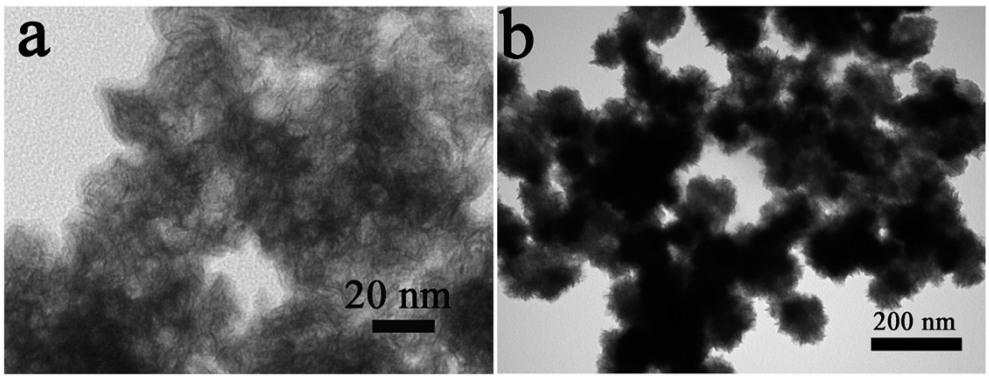

Fig. S10 TEM image of (a) the $ReSe_{2-x}$ nanosheets and (b) the $ReSe_2$ nanospheres after working as HER electrocatalyst for 12 hours (in 0.5 M H_2SO_4, overpotential of 250 mV).

Table. S3 Comparison of HER performance in acidic media for the current $ReSe_{2-x}$ nanosheets with other TMDC materials.

catalyst	Oneset overpotential (mV)	Current density (mA cm^{-2})	Corresponding overpotential (mV)	Tafel slope (mV/decade)	Reference
Se-vacant 1T' $ReSe_2$	50	10	102	67	This work
		100	249		
monolayer $ReSe_2$	~100	10	270	76	*Nano Research,* **2018**, *11,* 1787
Lithiated-1T' ReS_2	<100	>35	300	84	*Nano Lett.,* **2016**, *16*, 3780
1T' $ReSe_2$	80	8	300	67.5	*Electrochim., Acta* **2017**, *224*, 593
1T WS_2	80-100	0.02	150-175	60	*Nat. Mater.,* **2013**, *12*, 850
S-vacant	-	10	250	82	*Nat. Mater.,* **2016**, *15*,

2H MoS_2					48
1T WS_2	75	10	142	70	*Energy Environ. Sci.,* **2014**, *7*, 2608
Se-vacant 2H WSe_2	125	10	245	76	*Chem. Commun.,* **2016**, *52*, 14266
		150	400		
1T MoS_2	58	10	173	53	*Adv. Mater.,* **2018,** *30*, 1705509
1T $MoSe_2$	101		209	54	
1T WS_2	139		232	63	
1T $Mo_{0.5}W_{0.5}S_2$	95		196	58	
1T MoSSe	49		140	40	
1T MoS_2	-	10	271	61	*J. Am. Chem. Soc.,* **2018**, *140*, 441
1T/2H MoS_2	143	10	260	60	*Chem. Mater.,* **2017**, *29*, 7604
1T/2H $MoSe_2$	-	10	152	52	*Adv. Mater.,* **2017**, *29*, 1700311
Defected 2H $MoSe_2$	120	10	221	67	*Small,* **2017**, *13*, 1700565
2H $Mo_{1-x}W_xSe_2$	-	10	209	52	*Nanoscale,* **2017**, *9*, 13998
1T' $MoTe_2$	-	10	356	127	*2D Mater.,* **2017**, *4*, 025061
2H $MoTe_2$	-	10	650	184	
1T' WTe_2	-	10	430	57	*ACS Appl. Mater., Interfaces* **2018**, *10*, 458
2H $MoTe_2$	-	10	380	57	*ACS Catal.,* **2017**, *7*, 5706
P-1T-MoS_2		10	153	43	*J. Am. Chem. Soc.,* **2016**, *138,* 7965
Defected-MoS_2	-	16.3	350	108	*Chem. Commun.,* **2015**, *51,* 7470
2H $MoSe_{2-x}$	170	13	300	98	*Nanoscale,* **2014**, *6,* 11046

Table. S4 Comparison of HER performance of the $ReSe_{2-x}$ nanosheets with other catalysts systems.

catalyst	Oneset	Current	Corresponding	Tafel slope	Reference

	overpotential (mV)	density (mA cm^{-2})	overpotential (mV)	(mV/decade)	
Se-vacant 1T' $ReSe_2$	50	10	102	67	This work
		100	249		
MoS_2 /Graphene	~100	10	~150	41	*J. Am. Chem. Soc.* **2011**, *133*, 7296
Ni_2P nanoparticles	-	20	130	46	*J. Am. Chem. Soc.* **2013**, *135*, 9267
		100	180		
MoB	>100	20	210~240	55	*Angew. Chem. Int. Ed.* **2012**, *51*, 12703
Mo_2C				56	
porous-Mo_2C NW	70	10	200	53	*Energy Environ. Sci.*, **2014**, *7*, 387
NiO/Ni-CNT	-	100	<100	51	*Energy Environ. Sci.*, **2014**, *7*, 2608
FeP nanowire array/ Ti	16	10	55	38	*Angew. Chem. Int. Ed.* **2014** , *53*, 12855
		100	127		
MoP	50	30	180	54	*Energy Environ. Sci.*, **2014**, *7*, 2624
$Fe_{1-x}Co_xS_2$/ CNT	90	20	120	46	J. Am. Chem. Soc. **2015**, *137*, 1587
		100	170		
Porous C_3N_4 @N-Graphene	8	50	200	49	*ACS Nano*, **2015**, *9* , 931
NS-doped nanoporous graphene	130	10	390	80	*Angew. Chem. Int. Ed.* **2015**, *54*, 2131
NiCo2	-	10	104	59	*Adv. Mater.* **2017**, *29*, 1605502

P x					
$NiCo_2P_x$					
$NiCo_2S_4$N W/NF	-	10	210	58	*Adv. Funct. Mater.* **2016**, *26*, 4661
Single W Atom/ /N-Carbon	-	10	85	53	*Adv. Mater.* **2018**, *30*, 1800396
CoPS/CP	4	100	77	42	*J. Mater. Chem. A,* **2018**, *6*, 12353
M oS 2 /F N S/ Fe	30	10	122	45	*Adv. Mater.* **2018**, *30*, 1803151

Ni foam					
MoS_2/FNS/ FeNi foam					
hierarchical	120	10	230	72	*Angew.Chem.Int. Ed.* **2018**, *57,13302*

nanoporous graphene

hi
er
ar
ch
ic
al
na
n
o
p
or

o
us
gr
ap
he
ne

hierarchical
nanoporous
graphene

Additional References

S1. X. Zhou, J. Jiang, T. Ding, J. Zhang, B. Pan, J. Zuo and Q. Yang, *Nanoscale,* 2014, **6**, 11046-11051.

S2. Guo S and Sun S, *J. Am. Chem. Soc.*, 2012, **134**, 2492-2495.

S3. H. Vrubel and X. Hu, *Angew. Chem. Int. Ed.,* 2012, **51**, 12703-12706.

S4. C. Tang, N. Cheng, Z. Pu, W. Xing and X. Sun, *Angew. Chem. Int. Ed.,* 2015, **54***,*9351-9355.

S5. G. Kresse and J. Furthmüller, *Phys. Rev. B,* 1996, **54**, 11169-11186.

S6. G. Kresse and J. Furthmüller, *Comput. Mater. Sci.*, 1996, **6**, 15-50.

S7. J. P. Perdew, K. Burke and M. Ernzerhof, *Phys. Rev. Lett.,* 1996, *77*, 3865-3868.

S8. S. Grimme, *J. Comput. Chem.,* 2004, **25**, 1463-1473.

S9. S. Grimme, *J. Comput. Chem.,* 2006, **27**, 1787-1799.

S10. H. J. Monkhorst and J. D. Pack, *Phys. Rev. B*, 1976, **13**, 5188-5192.

S11. A. Arora, J. Noky, M. Drüppel, B. Jariwala, T. Deilmann, R. Schneider, R. Schmidt, O. D. Pozo-Zamudio, T. Stiehm, A. Bhattacharya, P. Krüger, S. M. de Vasconcellos, M. Rohlfing and R. Bratschitsch, *Nano Lett.,* 2017, **17**, 3202-3207.

S12. Q. Zhao, Y. Guo, Y. Zhou, X. Xu, Z. Ren, J. Bai and X. Xu, *J. Phys. Chem. C,* 2017, **121**, 23744-23751.

S13. J. K. Nørskov, T. Bligaard, A. Logadottir, J. R. Kitchin, J. G. Chen, S. Pandelov and U. Stimming, *J. Electrochem. Soc*., 2005, **152**, J23-J26.